Available online at www.sciencedirect.com
SCIENCE DIRECT®
Nuclear Instruments and Methods in Physics Research A 505 (2003) 645–655
NUCLEAR INSTRUMENTS & METHODS IN PHYSICS RESEARCH Section A
www.elsevier.com/locate/nima

Radiation tolerance of epitaxial silicon carbide detectors for electrons, protons and gamma-rays

F. Nava[a,*], E. Vittone[b], P. Vanni[c], G. Verzellesi[d], P.G. Fuochi[e], C. Lanzieri[f], M. Glaser[g]

[a] *INFN and Dipartimento di Fisica, Università di Modena e Reggio Emilia, Via G. Campi 213/A, I-41100 Modena, Italy*
[b] *Dipartimento di Fisica Sperimentale, Università di Torino, INFM-UniTo e INFN-To Italy*
[c] *CNR-Istituto LAMEL, Bologna, Italy*
[d] *INFM and DSI, Università di Modena e Reggio Emilia, Italy*
[e] *CNR-Istituto ISOF, Bologna, Italy*
[f] *Alenia Marconi Systems, Roma, Italy*
[g] *CERN, Division EP TA1-SD, Geneve, Switzerland*

Received 13 June 2002; received in revised form 6 August 2002; accepted 8 August 2002

Abstract

Particle detectors were made using semiconductor epitaxial 4H–SiC as the detection medium. The investigated detectors are formed by Schottky contact (Au) on the epitaxial layer and an ohmic contact on the back side of 4H–SiC substrates with different micropipe densities from CREE. For radiation hardness studies, the detectors have been irradiated with protons (24 GeV/c) at a fluence of about 10^{14} cm^{-2} and with electrons (8.2 MeV) and gamma-rays (^{60}Co source) at doses ranging from 0 to 40 Mrad. We present experimental data on the charge collection properties by using 5.48, 4.14 and 2.00 MeV α-particles impinging on the Schottky contact. Hundred percent charge collection efficiency (CCE) is demonstrated for reverse voltages higher than the one needed to have a depletion region equal to the α-particle projected range, even after the irradiation at the highest dose. By comparing measured CCE values with the outcomes of drift–diffusion simulations, values are inferred for the hole lifetime, τ_p, within the neutral region of the charge carrier generation layer. τ_p was found to decrease with increasing radiation levels, ranging from 300 ns in non-irradiated detectors to 3 ns in the most irradiated ones. The diffusion contribution of the minority charge carriers to CCE is pointed out.

PACS: 29.40.Wk; 78.70 − g

Keywords: Radiation hardness; Device simulation; Silicon carbide; Semiconductor detectors; Charge–particle spectroscopy

1. Introduction

It was shown that silicon carbide (SiC) is a useful material for the realisation of neutron [1] and charge particle [2–4] detectors, of dosimeters

*Corresponding author. Tel.: +39-059-20-55260; fax: +39-059-20-55235.
E-mail address: nava.filippo@unimo.it (F. Nava).

0168-9002/02/$ - see front matter
PII: S0168-9002(02)01558-9

[5] and of spectrometers [6], showing good performances and the potential of operating in high radiation damage environments [4–7] .

There has always been considerable interest in studying irradiation damage. This is due to its interesting physics as well as the technological importance.

High-energy particle bombardment, such as proton, neutron, electron and pion irradiation, as well as gamma-ray irradiation are often used [8–11].

Such an irradiation can create vacancies, interstitials and their associated defects. In a semiinsulating compound such as GaAs, antisites are also introduced [12,13].

These radiation-induced defects often have energy states in the band gap and therefore can strongly influence the detection properties like energy resolution and charge collection efficiency (CCE) [14–18].

In this article, we report our results of the α-particle response of simple pad detectors realised on 4H–SiC epitaxial layers grown by chemical vapour deposition (CVD), irradiated with 8.2 MeV electrons and gamma-rays from a ^{60}Co source up to a dose of 40 Mrad and with 24 GeV/c protons at a fluence of about 10^{14} p/cm^2.

2. Detector fabrication and experimental techniques

The SiC used in our experiments was 4H–SiC substrates of USA CREE Research Inc. Company with the following specifications.

- *For proton irradiated diodes*: wafer diameter 35 mm, thickness 0.32 mm, dopant nitrogen, net doping density of substrate 7×10^{18} cm^{-3}, standard micropipe density (101–200 cm^{-2}), n-type 30 μm thick epilayer with a typical net donor concentration, N_d–N_a, of 2.2×10^{15} cm^{-3}. Surface treatment: Si-face polished and C-face ground.
- *For electron and gamma-rays irradiated diodes*: wafer diameter 35 mm, thickness 0.36 mm, dopant nitrogen, net doping density of substrate 1×10^{18} cm^{-3}, selected micropipe density (10 cm^{-2}), n-type 30 μm thick epilayer with a typical net donor concentration, N_d–N_a, of 2.5×10^{15} cm^{-3}. Surface treatment: Si-face polished and C-face ground.

For all the diodes the ohmic contact, on the whole back of substrate (C-face), was obtained by the deposition of a 100 nm thick multilayer of Ti/Pt/Au followed by an annealing at 500°C for 30 s in argon ambient.

Before the fabrication of the Schottky barrier, after the standard cleaning in organic solvents, the native oxide layers on the Si surface of the epilayers were removed by a dry sputter etching with 200 eV argon ions. The thin film of gold was deposited on the epilayer by the RF magnetron sputtering method at room temperature. The circular dots were made by photolitography.

Diameter and thickness of Au contacts were 2 and 100 nm, respectively.

The wafers were then cut into 5×5 mm^2 samples which were fixed by a conducting silver glue paint on the test fixture and contacted by a gold wire and a conducting silver paint for the electrical characterisation and detection properties measurements.

The irradiation was carried out at 26°C in the T7 beam at the CERN–Proton Synchrotron (CH) with 24 GeV/c protons and at ISOF-CNR (Italy) laboratory with 8.2 MeV electrons of a LINAC accelerator and with gamma-rays from a ^{60}Co source [19].

The quality of each Schottky diode was evaluated before and after irradiation in terms of the measured ideality factor n and the barrier height ϕ_b, using standard current–voltage (I/V) and capacitance–voltage (C/V) techniques in the dark and at room temperature.

The detector performances have been tested by α-particles of three different energies: 5.48, 4.14 and 2.00 MeV. The 5.48 MeV α-particles were obtained from an ^{241}Am source in vacuum (about 1 Pa) whereas the 4.14 MeV ones were obtained by decelerating the ^{241}Am α-radiation in air. The 2.00 MeV α-particles were obtained by using the He^+ ion beam at the facility of Italian National

Laboratory of Legnaro (INFN) under high vacuum conditions ($<10^{-3}$ Pa).

The CCE was measured by a standard procedure, which normalises the pulse height with respect to the response obtained in the same experimental condition of an Si p/n junction detector with the energy needed to produce one electron–hole pair being 3.60 and 8.40 eV in Si and SiC, respectively.

3. Experimental results

3.1. Proton irradiated diodes

A schematic cross-section of the Schottky diode structure is shown in Fig. 1.

3.1.1. I/V curves

The room temperature forward and reverse I/V characteristics of the Schottky diode, before and after irradiation, are reported in Fig. 2(a) and (b), respectively.

Good linear behaviour over at least eight decades is observed in the log(I) versus V_{forward} plot. The ideality factor, n, is extracted from the slope of the linear part and a value of about 1.18 is found both before and after irradiation, suggesting

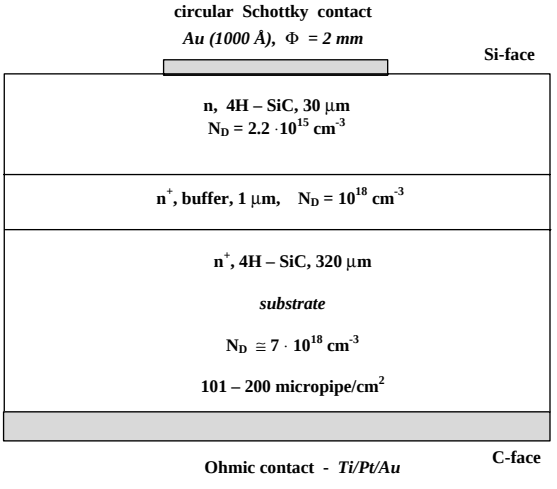

Fig. 1. Scheme of the detectors used in the present work for proton irradiation study.

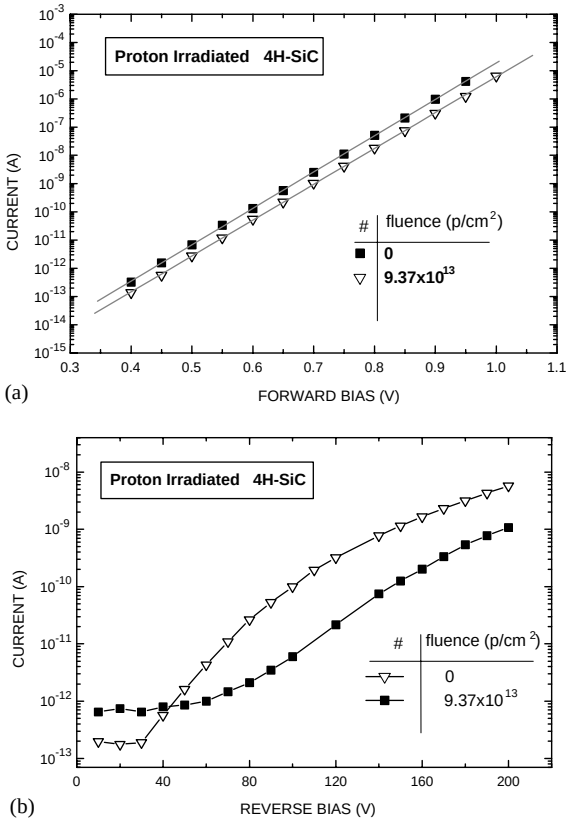

Fig. 2. Current versus (a) forward and (b) reverse applied voltage for Schottky diodes non-irradiated and 24 GeV/c proton irradiated at the indicated fluence at room temperature.

an excess current from recombination in the depletion region or at the interface states or at an intermediate insulating layer.

On the contrary, a remarkable change in the reverse current is observed after irradiation: at high reverse voltage, the current decreases by almost one decade with the irradiation in opposite to what has been observed in Si [20,21] and GaAs [22,23] Schottky diodes.

3.1.2. C/V curves

Fig. 3 shows the reciprocal of the squared capacitance ($1/C^2$) per unit area as a function of the bias. The barrier height , ϕ_b, and the effective dopant concentration, N_{eff}, are inferred from the extrapolated intercept on the voltage axis and from the slope of the straight line, respectively [24]. All measured data were extracted from 1 to 6 V

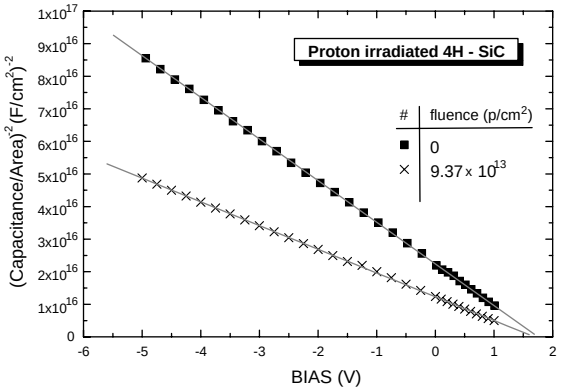

Fig. 3. $1/C^2$ versus applied voltage for the Schottky diodes of Fig. 2 at room temperature.

Table 1
Results of Schottky barrier height ϕ_b, ideality factor n and effective dopant concentration N_{eff} measurements by I/V and C/V methods for 24 GeV/c proton irradiated diodes at the indicated fluences

Fluence	0	9.37×10^{13} p/cm^2
N_{eff} (cm^{-3})	2.18×10^{15}	1.43×10^{15}
Φ_b (eV)	1.70	1.72
n	1.19	1.18

range in order to study the depletion capacitance near the metal–semiconductor interface and are reported in Table 1. The regression coefficient was always better than 0.999.

While ϕ_b remains constant, N_{eff} is found to decrease with the irradiation, suggesting a partial compensation of the nitrogen atoms by the generated intrinsic defects.

3.1.3. Charge collection

Fig. 4 shows the experimental CCE versus $V_{reverse}$ curves of proton irradiated detectors for 5.48, 4.14 and 2.00 MeV α-particles. The corresponding Bragg ionisation curves, as obtained from SRIM2000 simulation [25], are reported in Fig. 5.

The following comments can be made:

(1) in all cases, increasing the reverse bias widens the diode depletion region and therefore increases the CCE, as more energy is deposited in the high electric field region where the generated charges are collected more efficiently;
(2) in the case of 4.14 and 2.00 MeV α-particles, the CCE reaches almost 100% at $V_{reverse} \geqslant 170$ and 40 V, respectively, as the depleted region entirely contains the particle generation tracks.

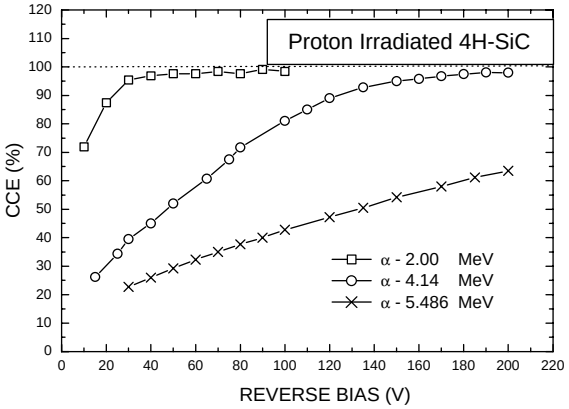

Fig. 4. Experimental CCE values for 5.48, 4.14 and 2.00 MeV α-particles impinging on the Schottky contact of the proton irradiated diodes of Fig. 2, versus reverse bias at room temperature.

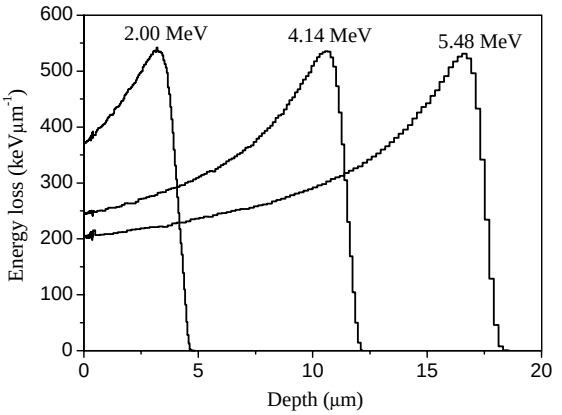

Fig. 5. Bragg ionisation curves of 5.48, 4.14 and 2.00 MeV α-particles in SiC.

It must be stressed that even after the proton irradiation at the mentioned fluence, all the generated charges are collected. On the contrary, the best Si [26] and GaAs [27] detectors irradiated

with 24 GeV/c proton at this fluence, show a decrease of CCE in the order of 10–15% at the same values of the electric field in the depleted region.

3.2. Electron and gamma-ray irradiated diodes

A schematic cross-section of the Schottky diode structure is shown in Fig. 6. Two diodes with such a structure have been irradiated in subsequent times at the following doses: 2, 10, 20 and 40 Mrad with 8.2 MeV electrons and gamma-rays from a ^{60}Co source, respectively. The tests have been performed after each irradiation.

3.2.1. I/V curves

The room temperature forward and reverse I/V characteristics of the Schokky diodes, before and after electron irradiation, are reported in Figs. 7(a) and (b), respectively. Only the data of the diodes irradiated at the highest doses of 20 and 40 Mrad are shown, since they are the more significant ones.

Even after irradiation, a good linear behaviour over eight decades is observed in the log (I) versus V_{forward} plot. A value of 1.03 was extracted from the slope for the ideal factor independently of the irradiation, indicating that, in these diodes, the thermoionic emission is the most significant contribution to the current across the barrier.

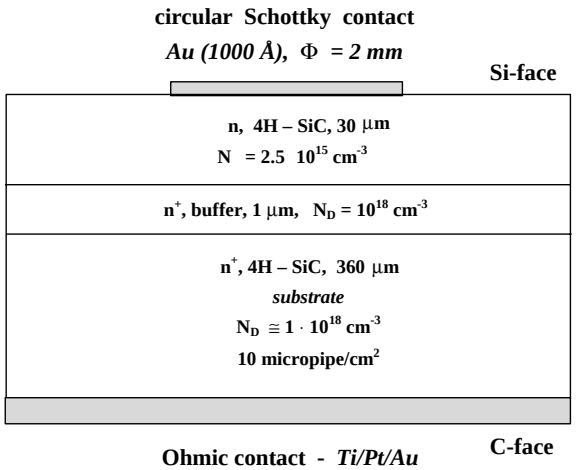

Fig. 6. Scheme of the detectors used in the present work for electron and gamma-rays irradiation study.

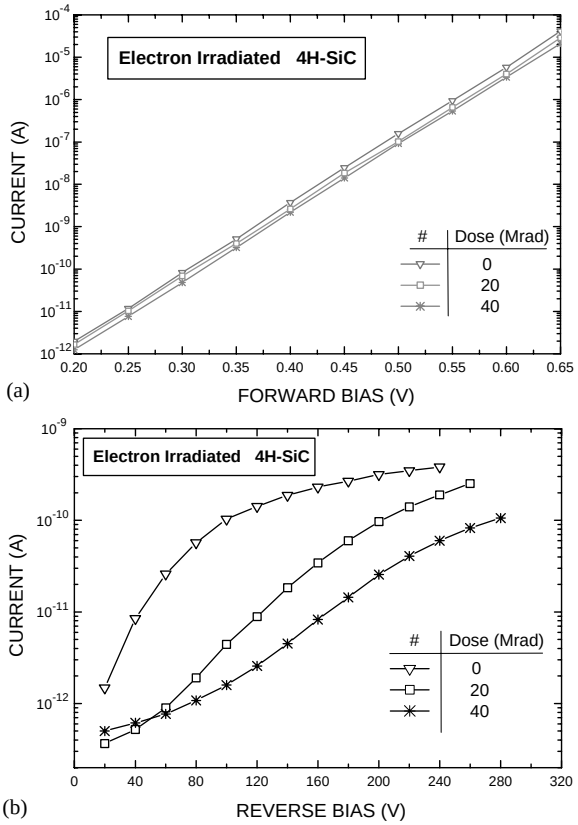

Fig. 7. Current versus (a) forward and (b) reverse applied voltage for Schottky diodes non-irradiated and 8.2 MeV electron irradiated at the indicated doses at room temperature.

Again, as for the proton irradiated Schottky diodes, a remarkable decrease of the reverse current is observed after irradiation.

Figs. 8(a) and (b) report forward and reverse I/V curves for the non-irradiated diode and after the irradiation with gamma-rays at 20 and 40 Mrad, respectively. No difference was observed in the forward polarisation, while in the reverse bias condition a slight decrease in the current was observed at the lowest voltages and at the highest dose. The same value, 1.03, was found for the ideality factor, independently from the dose.

3.2.2. C/V curves

Figs 9(a), (b) and (c) show the reciprocal of the squared capacitance per unit area as a function of the bias for the non-irradiated diode and after the

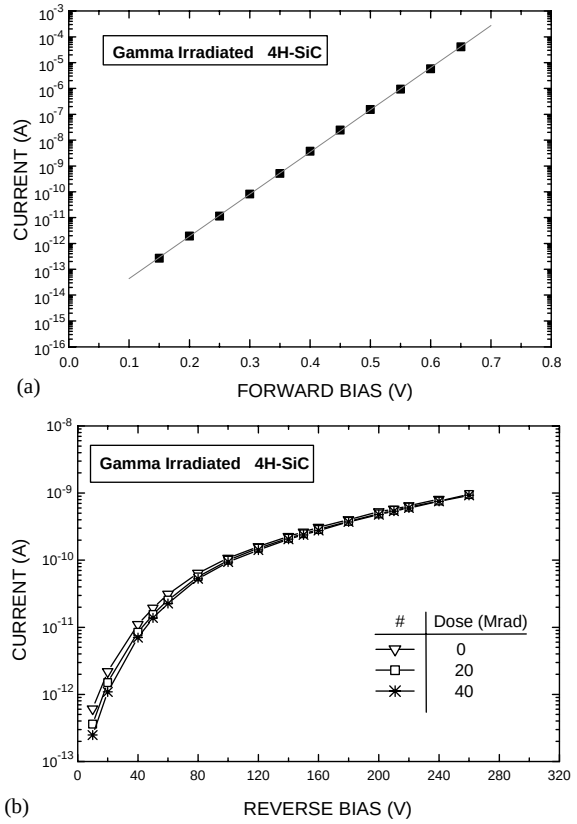

Fig. 8. Current versus (a) forward and (b) reverse applied voltage for Schottky diodes non-irradiated and gamma from ^{60}Co source irradiated at the indicated doses at room temperature.

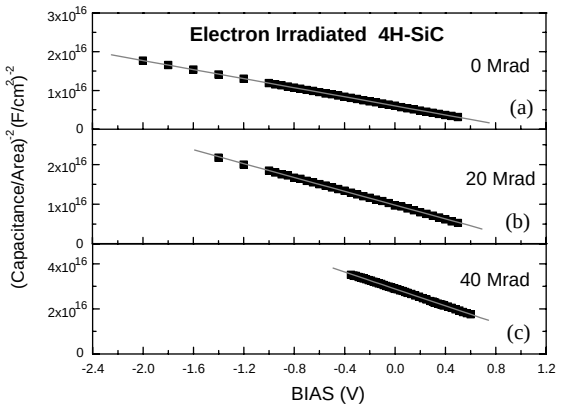

Fig. 9. $1/C^2$ versus applied voltage for the Schottky diodes of Fig. 7.

Table 2
Results of ϕ_b, n and N_{eff} measurements by current–voltage (I/V) and capacitance–voltage (C/V) methods for 8.2 MeV electron irradiated; and gamma-rays irradiated diodes at the indicated doses

8.2 MeV electron irradiation			
Dose (Mrad)	0	20	40
N_{eff} (cm^{-3})	2.49×10^{15}	1.67×10^{15}	6.89×10^{14}
Φ_b (eV)	1.03	1.13	1.54
n	1.034	1.036	1.032
Gamma irradiation from ^{60}Co			
Dose (Mrad)	0	20	40
N_{eff} (cm^{-3})	2.49×10^{15}	2.28×10^{15}	2.21×10^{15}
Φ_b (eV)	1.03	1.03	1.03
n	1.034	1.033	1.034

electron irradiation at the more significant doses of 20 and 40 Mrad, respectively. The data of ϕ_b and N_{eff} were extracted from appropriate bias ranges, with a regression coefficient always better than 0.999, in order to study the depletion capacitance near the metal–semiconductor interface and are reported in Table 2.

The same analysis was done for gamma-irradiated Schottky diodes. The relative curves are reported in Figs. 10(a), (b) and (c) for 0, 20 and 40 Mrad, respectively, while the extracted data for ϕ_b and N_{eff} are reported in Table 2.

These results put into evidence that:

(a) the electron irradiation influences drastically the reverse conduction, the Schottky barrier and the net dopant concentration in the epilayer. N_{eff} and the reverse current were found to decrease with the dose, while ϕ_b was found to increase with the dose;
(b) in the gamma-irradiated diodes, while ϕ_b remains constant, N_{eff} decreases slightly with the doses;
(c) the ideality factor values do not change with the dose neither in electron nor in gamma-irradiated Schottky diodes;
(d) the range of the linear behaviour decreases with increasing the dose in the electron irradiated diodes, while it does not change in the gamma-irradiated ones.

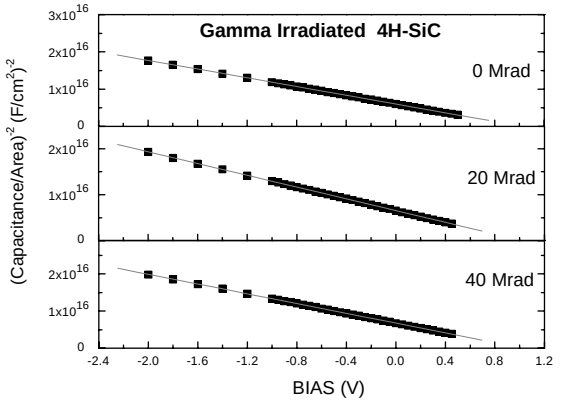

Fig. 10. $1/C^2$versus applied voltage for the Schottky diodes of Fig. 8.

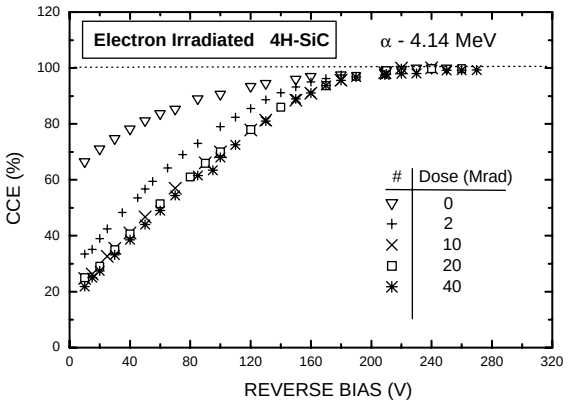

Fig. 11. Experimental CCE values for 4.14 MeV α-particles impinging on the Schottky contact of diodes irradiated by 8.2 MeV electrons at the indicated doses at room temperature.

3.2.3. Charge collection

The diodes have been tested as radiation detectors by irradiating the Schottky contact with 4.14 MeV α-particles.

Figs. 11 and 12 report the data of CCE for non-irradiated and electron/gamma-irradiated diodes at the indicated doses, respectively.

Several important features are to be pointed out:

(i) the CCE decreases with the dose, with data showing an initial fast fall at 2 Mrad followed by a slower fall rate at higher doses. This behaviour is more pronounced in the case of electron irradiation, where the CCE data taken at 20 and 40 Mrad are almost equal.

(ii) independently on the radiation level, the CCE saturates at 100% at reverse bias values above the one necessary to have a depleted region equal to the α-particle projected range.

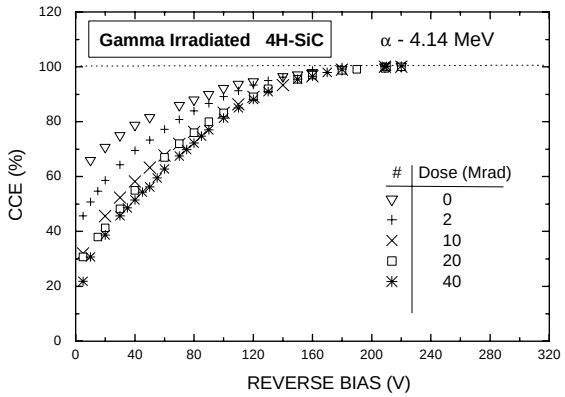

Fig. 12. Experimental CCE values for 4.14 MeV α-particles impinging on the Schottky contact of diodes irradiated by gamma-rays at the indicated doses at room temperature.

4. Charge collection analysis

To gain deeper insight into the charge collection properties of the Schottky radiation detectors, the experimental CCE data are compared with the theoretical CCE versus V_{reverse} curves obtained by using the drift–diffusion semiconductor-device analysis program DESSIS [28] and/or a simple drift–diffusion analytical expression [29]. This latter model evaluates the charge collection efficiency by the following expression:

$$\mathrm{CCE} = \frac{1}{E_{\text{ion}}}\int_0^W \frac{\mathrm{d}E}{\mathrm{d}x}\,\mathrm{d}x + \frac{1}{E_{\text{ion}}}\int_W^R \frac{\mathrm{d}E}{\mathrm{d}x}\,\mathrm{e}^{-\frac{(x-W)}{L_{\text{p}}}}\,\mathrm{d}x \qquad (1)$$

where E_{ion} is the ion energy, $\mathrm{d}E/\mathrm{d}x$ is the electronic stopping power, R is the penetration depth of ions, L_{p} is the hole diffusion length and W is the depletion layer width as determined by C/V measurements. The first term of Eq. (1) represents the charge collected from the depletion

region where fast charge carriers drift under the influence of the electric field and, assuming the drift time shorter than the carrier lifetime, where the complete charge collection occurs. The second term of Eq. (1) represents the charge collected from the diffusion region. This term is obtained integrating in time the net diffusion current of holes that arrive at the interface at depth W, considering an integration time (amplifier shaping time) much longer than the hole lifetime [30]. L_p can be evaluated by solving a system of integral equations (1) where CCE is given by the centroid position of the spectra measured at different ion energies and bias voltages and the stopping power is given by SRIM2000 simulation.

Material and transport related parameters were customised to 4H–SiC using values taken from the literature [31].

4.1. Proton irradiated detectors

For proton irradiated detectors, the CCE experimental data were fitted by using both the methods.

Fig. 13 compares the experimental CCE data with the theoretical values derived from the numerical simulation using the value of 3.00 ns for the hole life time, τ_p. In the inset, the fit parameters are reported.

In Fig. 14, the CCE experimental data are compared to best-fit curves obtained by a minimising root-mean-square deviation (rms) procedure and by allowing the fit parameter hole diffusion length, L_p, to float in the drift–diffusion analytical expression.. The value of L_p ($L_p = (D_p\tau_p)^{1/2}$), which minimises the rms error, was found to be 1.01 μm, which corresponds, by combining with the Einstein relationship $D_p = (kT/q)\,\mu_p$ [24], to $\tau_p = 3.31$ ns in good agreement with the one inferred as outcome of the DESSIS simulation. In the same figure, the drift and diffusion contributions to the total charge collection are reported.

These results put into evidence that:

(i) also after irradiation to the highest dose (40 Mrad) the measured CCE values exceed those predicted by neglecting the contribution of the minority carrier diffusion, until the depletion region becomes wider than the α-particle penetration depth and CCE becomes unity;

(ii) the CCE values can be well interpreted by using a less time consuming best fit procedure and the drift–diffusion analytical expression (1);

(iii) the analytical drift–diffusion model assumes that the interaction of the ion with the semiconductor does not significantly perturb

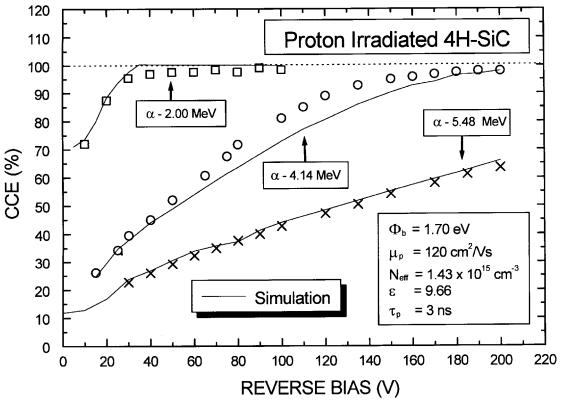

Fig. 13. CCE data of Fig. 4 compared with the outcomes of drift–diffusion simulations performed by means of the semiconductor-device analysis program DESSIS. The fit parameters, Schottky barrier ϕ_b, hole mobility μ_p, effective dopant concentration N_{eff}, hole life time τ_p and dielectric constant ε, are reported in the inset.

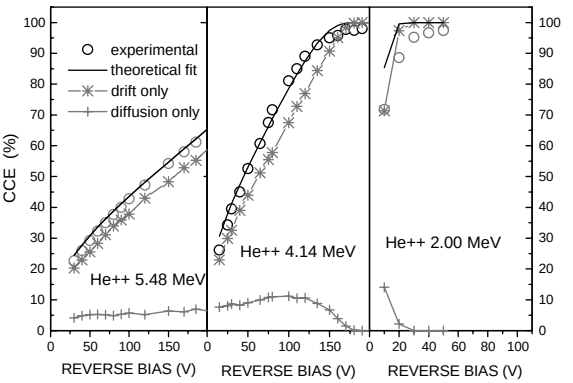

Fig. 14. CCE data of Fig. 4 compared with best-fit curves obtained with the value of 1.01 μm for the best-fit parameter L_p in the drift–diffusion analytical expression. The drift-only CCE and diffusion-only CCE curves are also reported.

the electric field within the material, i.e. when plasma or funneling effects are not present. Such a consideration can explain the decreasing goodness of fit as the ion energy decreases, i.e. as the density of charge carriers along the ion track increases up to generate plasma effects [30].

4.2. Electron irradiated detectors

For electron and gamma-irradiated detectors, the CCE experimental data were interpreted by using the best fit procedure with the drift–diffusion analytical expression, only.

In Fig. 15 these data, acquired with 4.14 MeV α-particles, are compared to best fit curves for the non-irradiated detectors (a) and electron irradiated detectors at 2 Mrad (b) and 40 Mrad (c). In the same figure the drift and diffusion contributions to the total charge collection are reported.

The following important comments can be made:

(i) a remarkable decrease of hole diffusion length L_p is observed with the dose. L_p was found to degrade from 9.5 μm ($\tau_p = 303$ ns) for unirradiated detectors to 2 μm ($\tau_p = 13$ ns) and to 1.00 μm ($\tau_p = 3.30$ ns) for electron irradiated detectors at 2 and 40 Mrad, respectively;

(ii) such a degradation, which can be ascribed to the creation of defects during the electron exposure, seems to disappear when the high electric field extends within the neutral region of the charge carrier generation with increasing $V_{reverse}$. In other words the induced defects, acting as hole trapping centres, are much more less effective in the high electric field regions.

4.3. Gamma-irradiated detectors

In Fig. 16, the CCE experimental data, acquired with 4.14 MeV α-particles, are compared to best fit curves for non-irradiated detectors (a) and gamma-irradiated detectors at 2 Mrad (b) and 40 Mrad (c), respectively. In the same figure, the drift and diffusion contributions to the total CCE are reported.

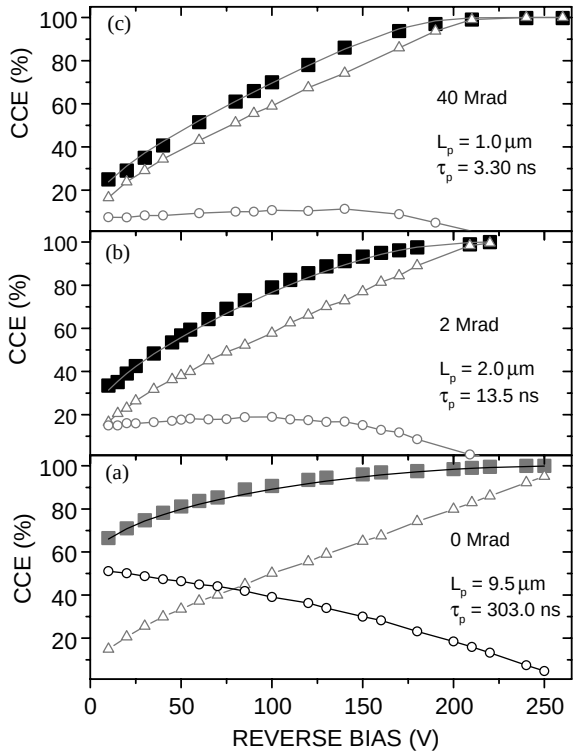

Fig. 15. CCE data of Fig. 11 at the doses of (a) 0, (b) 2 and (c) 40 Mrad compared with the best-fit curves (—) obtained with the indicated best-fit values for L_p in the drift–diffusion analytical expression. The drift (Δ) and diffusion (◦) contribution curves are also reported.

These interpretations demonstrate that (i) an important contribution to CCE curves arises from the carriers generated in the neutral region and diffusing to the junction also in detectors irradiated at the highest dose (40 Mrad) and (ii) the aforesaid contribution decreases with increasing the dose. L_p was found to degrade from 9.9 μm ($\tau_p = 329.0$ ns) for non-irradiated detectors, to 5 ($\tau_p = 84.4$ ns) and 1.6 μm ($\tau_p = 8.4$ ns) for gamma-irradiated detectors at 2 and 40 Mrad, respectively.

5. Discussion and conclusion

Schottky diodes have been realised by using the same process, on n-type 4H–SiC undoped epitaxial

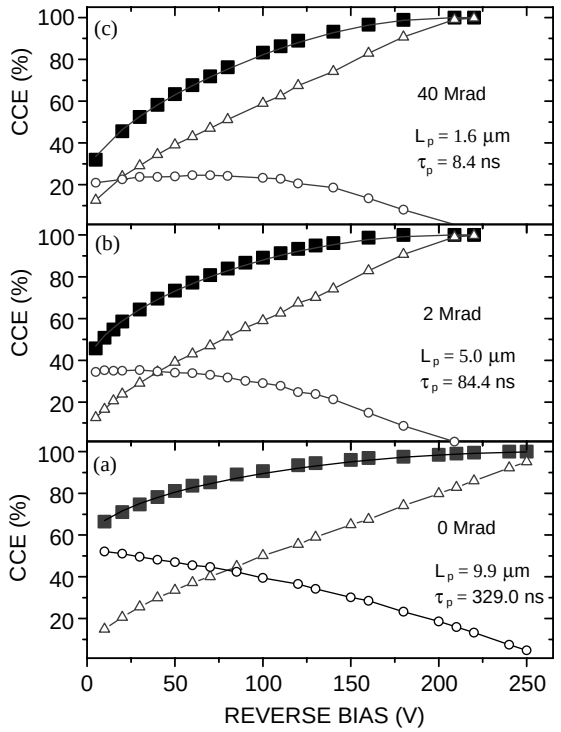

Fig. 16. CCE data of Fig. 12 at the doses of (a) 0, (b) 2 and (c) 40 Mrad compared with the best-fit curves (—) obtained with the indicated best-fit values for L_p in the drift–diffusion analytical expression. The drift (Δ) and diffusion (◦) contribution curves are also reported.

layers, 30 μm thick, grown by CVD on 4H–SiC substrates with a content of micropipes ranging from 101–200 to 10 cm^{-2}, as claimed by CREE, respectively. Typical net donor concentration, N_d–N_a, in the n layer was 2.2–2.5 × 10^{15} cm^{-3}.

The diodes have been irradiated at room temperature with 24 GeV/c protons at a fluence of about 10^{14} cm^{-2} and with 8.2 MeV electrons and gamma at different doses up to 40 Mrad.

The different value of the micropipe density was found to play an important role on the Schottky barrier (SBH) formation and the electrical transport mechanism across it.

The diodes, realised on substrates characterised by the higher micropipe density, show indeed values for the SBH and the reverse current and a departure from unity for the ideality factor higher than the ones obtained with diodes realised on lower micropipe density substrates.

Concerning the SBH value, the irradiations play also a different effect: negligible in diodes realised on substrates with an high micropipe density, remarkable in the other ones.

A common effect of the irradiation was observed in all the diodes independently of the crystallographic quality of the substrate and type of irradiation: the decrease of N_{eff} and the reverse current with increasing the dose. Since the proton and electron irradiation was found to lead to the formation of both donor and acceptor deep centres [32–34], we believe that these centres can reduce the effective doping by the compensation of the nitrogen donors and consequently the base conductivity at room temperature. Moreover, in the electron irradiated diodes this mechanism is not uniform in depth starting from the Schottky contact, indicating a non-uniform generation of these centres during the room temperature electron irradiation.

These behaviours, however, are quite complex and additional research is needed in order to interpret them and confirm the above-mentioned speculations.

The nuclear response, evaluated with 5.48, 4.14 and 2.00 MeV α-particles, showed a complete collection (CCE = 1) for all the irradiated diodes and independently of the crystallographic quality of the 4H SiC substrate, measured by the micropipe density value, on top of which the epitaxial layers were grown by CVD. By fitting the measured CCE with drift–diffusion simulations, the contribution to the CCE of the diffusion of the minority carriers generated outside the depletion region (the neutral one), was found to be present also in the detectors irradiated at the highest levels.

The relatively high value of 300 ns obtained for the minority carrier life time, τ_p, in non-irradiated detectors, corresponding to a diffusion length of about 9 μm, was shown to degrade to about 3 ns in the detectors irradiated at the highest doses. This remarkable decrease can be ascribed to the minority carrier traps induced by the irradiation and to the absence of the electric field in the neutral region.

DLTS, MCTS and EBIC analysis are in progress for determining the trapping centres which play the main role in the degradation of

the detection parameters and to measure the effect of the electric field on τ_p.

Acknowledgements

This work was partially supported by Istituto Nazionale di Fisica Nucleare (INFN) and by MIUR cofin2001 (Italy).

References

[1] A.R. Dullo, et al., IEEE Trans. Nucl. Sci. NS-46 (1999) 275.
[2] F.H. Ruddy, et al., IEEE Trans. Nucl. Sci. NS-45 (1998) 536.
[3] F. Nava, et al., Mater. Sci. Forum 353–356 (2001) 757.
[4] M. Rogalla, et al., Nucl. Phys. B (Proc. Suppl.) 78 (1999) 520.
[5] M. Bruzzi, et al., Diamond Rel. Mater. 10 (2001) 657.
[6] G. Bertuccio, et al., IEEE Trans. Nucl. Sci. NS-48 (2001) 232.
[7] S. Seshadri, et al., IEEE Trans. Nucl. Sci. NS-46 (1999) 567.
[8] W. Karpinski, et al., Nucl. Instr. and Meth. A 323 (1992) 635.
[9] M. Rogalla, et al., Nucl. Instr. and Meth. A 395 (1997) 45 and references therein.
[10] W. Braunschweig, et al., Nucl. Instr. and Meth. A 372 (1996) 111.
[11] F. Lemeilleur, et al., Nucl. Instr. and Meth. A 360 (1995) 438 and references therein.
[12] M. Rogalla, et al., Nucl. Instr. and Meth. B 134 (1998) 53.
[13] P. Vanni, et al., Nucl. Phys. B (Proc. Suppl.) 78 (1999) 521.
[14] F. Nava, et al., Nucl. Instr. and Meth. A 426 (1999) 185.
[15] U. Biggeri, et al., Nucl. Phys. B, Proc. Suppl. 78 (1999) 527.
[16] M. Rogalla, et al., Nucl. Instr. and Meth. A 410 (1998) 41.
[17] F. Lemeilleur, G. Lindström, S.J. Watts, Third ROSE Workshop on Radiation Hardening of Silicon Detectors, 12–14 February 1998, DESY Proceedings, Hamburg University, Germany.
[18] T.E. Schlesinger, et al., Mater. Sci. Eng. 32 (2001) 103 Reports and references therein.
[19] P.G. Fuochi, Radiat. Phys. Chem. 44 (1994) 431.
[20] S.J. Bates, Ph.D. Thesis, Cambridge University, 1994 (Chapter 5).
[21] F. Lemeilleur, et al., IEEE Trans. Nucl. Sci. NS-41 (1994) 425.
[22] U. Biggeri, et al., Nucl. Phys. B (Proc. Suppl.) 78 (1999) 527.
[23] Th. Kubicki, et al., Nucl. Phys. B (Proc. Suppl.) 44 (1995) 528.
[24] S.M. Sze, Physics of Semiconductor Devices, 2nd Edition, Wiley, New York, 1981.
[25] J.F. Ziegler, et al., Transport of ions in Matter, Pergamon Press, New York, 1985.
[26] C. Leroy, et al., Paper presented at the International Conference. on Radiation Effects on Semiconductor Materials, Detectors and Devices, Florence, 6–8 March, 1996.
[27] F. Nava, et al., IEEE Trans. Nucl. Sci. NS-44 (1997) 943.
[28] G. Verzellesi, et al., Nucl. Instr. and Meth. A 476 (2002) 717.
[29] M. Jaksic, et al., Nucl. Instr. and Meth. B 188 (1–4) (2002) 130.
[30] E. Vittone, et al., Nucl. Instr. and Meth. B 161–193 (2000) 446 and references therein.
[31] C.E. Weitzel, et al., IEEE Trans. Electron. Dev. ED-43 (10) (1996) 1732.
[32] L. Storasta, et al., Mater. Sci. Forum 353–0356 (2001) 431 and references therein.
[33] H.J. von Bardeleben, J.L. Cantin, Mater. Sci. Forum 353–356 (2001) 513 and references therein.
[34] V. Ya Bratus, et al., Mater. Sci. Forum 353–356 (2001) 517.